IMAGE SEGMENTATION WITH DYNAMIC ARTIFACTS DETECTION AND BIAS CORRECTION

DOMINIQUE ZOSSO[1], JING AN, JAMES STEVICK, NICHOLAS TAKAKI, MORGAN WEISS

University of California, Los Angeles, Department of Mathematics
520 Portola Plaza, Box 951555, Los Angeles, CA 90095-1555, USA

LIANE S. SLAUGHTER, HUAN H. CAO, PAUL S. WEISS

University of California, Los Angeles, California NanoSystems Institute (CNSI)
570 Westwood Plaza, Building 114, Los Angeles, CA 90095, USA
University of California, Los Angeles, Department of Chemistry and Biochemistry
607 Charles E. Young Drive, Los Angeles, CA 90095, USA
University of California, Los Angeles, Department of Materials Science and Engineering
410 Westwood Plaza, Los Angeles, CA 90095, USA

ANDREA L. BERTOZZI

University of California, Los Angeles, Department of Mathematics
520 Portola Plaza, Box 951555, Los Angeles, CA 90095-1555, USA

(Communicated by the associate editor name)

ABSTRACT. Region-based image segmentation has essentially been solved by the Chan-Vese (CV) model. However, this model fails when images are affected by artifacts (outliers) and illumination bias that outweigh the actual image contrast. Here, we introduce a model for segmenting such images. In a single energy functional, we introduce 1) a dynamic artifact class preventing intensity outliers from skewing the segmentation, and 2), in Retinex-fashion, we decompose the image into a piecewise-constant structural part and a smooth bias part. The CV-segmentation terms then only act on the structure, and only in regions not identified as artifacts. The segmentation is parameterized using a phase-field, and efficiently minimized using threshold dynamics.

We demonstrate the proposed model on a series of sample images from diverse modalities exhibiting artifacts and/or bias. Our algorithm typically converges within 10-50 iterations and takes fractions of a second on standard equipment to produce meaningful results. We expect our method to be useful where image damage prevents classical CV-segmentation from working, and anticipate use in applications where artifacts and bias are actual features of interest, such as lesion detection and bias field correction medical imaging, e.g. in magnetic resonance imaging (MRI).

1

1. **Introduction.** Image segmentation is the task of partitioning the image domain Ω into homogeneous regions corresponding to individual objects, $\Omega = \sqcup_i \Omega_i$, or by duality, to find the contours Γ that define the boundaries $\partial \Omega_i$ of these objects. Image segmentation is most commonly formulated variationally as a minimization problem, where one optimizes a parameterization of the regions or their contours towards specific segmentation criteria encoded in the objective functional. Fundamental image segmentation models underlying the two respective segmentation goals are snakes [19] or geodesic active contours (GAC) [5] for edge-based segmentation, and active contours without edges (ACWE, a.k.a. Chan-Vese or CV model) [7] for region-based segmentation. For both GAC and CV, the segmentation can conveniently be parameterized implicitly using the level set method [34], and various efficient optimization schemes have been presented, e.g. [9, 27, 3, 15].

Here, we are interested in region-based image segmentation, and improvements to the CV model in particular, to segment images that are affected by both image artifacts (single or grouped outliers such as scars, occlusions, scratches) and illumination bias (gain inhomogeneity, shadows). Examples of such images are found in atomic force microscopy (AFM), where these image imperfections are due both to the samples and the image acquisition, in infrared imaging, which suffers from noise and gain inhomogeneity, as well as in medical imaging modalities such as magnetic resonance imaging (MRI; bias field inhomogeneity, coil sensitivity, lesions). In some applications, artifacts (and outliers) are not only a nuisance but the actual object of interest, such as in lesion and tumor detection in brain MRI [35], or exploration in geochemistry [16].

The CV model is initially derived from the Mumford-Shah functional (MS) [32], which from an input image $I_0 \colon \Omega \subset \mathbb{R}^n \to \mathbb{R}$ recovers an image $I \colon \Omega \to \mathbb{R}$ to be smooth almost everywhere:

$$E_{\mathrm{MS}}(I, \Gamma) = \int_\Omega (I - I_0)^2 + \alpha \int_{\Omega \setminus \Gamma} |\nabla I|^2 + \beta \int_\Gamma, \tag{1}$$

where the three terms aim towards data fidelity, smoothness, and short boundary length; $\Omega \subset \mathbb{R}^n$ is the entire image domain and $\Gamma \subset \Omega$ the boundary set of Hausdorff dimension $n-1$ where the approximation I exhibits discontinuities. Indeed, the CV model is defined as the *cartoon-limit* ($\alpha \to \infty$) of the MS functional, where the recovered image is required to be piecewise constant, and regions are thus characterized by a single representative color each, μ_i:

$$E_{\mathrm{CV}}(\mu_i, \Omega_i) = \sum_i \lambda_i \int_{\Omega_i} (\mu_i - I_0)^2 + \beta/2 \sum_i \int_{\partial \Omega_i}, \tag{2}$$

with λ_i and β being parameters. The representative colors μ_i are to be determined along with the optimal image domain partitioning $\Omega = \sqcup_i \Omega_i$.

The reduction of the segmentation model to two phases and using the level-set representation of these two phases leads to the following classical formulation [7]:

$$E_{\mathrm{CV}}(\mu_1, \mu_2, \phi) = \lambda_1 \int_\Omega (\mu_1 - I_0)^2 H(\phi) + \lambda_2 \int_\Omega (\mu_2 - I_0)^2 (1 - H(\phi)) + \beta \int_\Omega |\nabla H(\phi)|, \tag{3}$$

where the levelset function ϕ is positive in object regions, negative in background regions, zero on the object boundaries, and H is the Heaviside function. The last term represents the total variation of the characteristic function of the object, $H(\phi)$, and is the co-area-formula equivalent of the boundary length term.

The Chan-Vese active contour model has seen a number of specific modifications. For example, while the initial model could only segment greyscale images into two regions, the authors have extended it to adapt to vector-valued images [10], and they have also illustrated an extension of the model to multi-phase segmentations [39]. Unfortunately, all of these models often fail to segment images which feature damage, such as artifacts and

bias. Occlusion of objects, scars, and other artifacts on the image, and images featuring regional color inhomogeneity challenge CV and CV-like segmentation models. Several models propose partial solutions.

Regarding images affected by artifacts, Jung, Kang, and Kang [18] created an L^1 variant of the CV scheme, which is more robust to outliers, along with a numerical scheme to minimize it. Indeed, the original quadratic fidelity term in the CV model corresponds to a Gaussian additive noise prior on top of the piecewise constant image model [4]. Impulsive noise or other outliers, in particular due to image artifacts, therefore overly impact the functional and skew the image statistics μ_i, against which the L^1-term is more robust.

To deal with illumination bias, one could remove regional color inhomogeneity as a preprocessing step, or build a model which explicitly incorporates non-constant piecewise regions. An example of the former is an L^1-Retinex model [28, 43, 44], which gathers the piecewise-constant (or relatively constant) structure of an image by removing the smooth bias field. Retinex models remove shadows, but do not guide their corrections to the segmentation. On the other hand, Li et al. [24] propose a region-scalable fitting model which replaces the piecewise constant requirement of the CV model with a local averaging fidelity term which decreases penalty from distant points. This is effectively a partial roll-back from the CV cartoon-limit of the MS-model insofar as regions are not required to be piecewise flat, but piecewise smooth, only. Wang et al. [40] apply this model to medical imaging with success, while Yang et al. [42] use the split Bregman method to expedite segmentation. As illustrated in their papers, the model was able to identify inhomogeneous regions, but, in our experience, the algorithm has trouble when objects are sparse and disconnected. Moreover, the region-scalable fitting model is unable to effectively deal with artifacts.

Another (unspecific) approach is to use some prior knowledge of the object region's shape to guide the segmentation and overcome difficulties with pure intensity cues, e.g. [36, 13, 8, 12]. In all cases, these models are able to use shape information to guide the segmentation, but require an accurate shape prior to work with. Moreover, aligning this shape prior can be computationally expensive, or require supervision.

In this paper, we propose a new model which dynamically identifies artifacts and corrects shadows during the segmentation. The principal goal is to formulate an image segmentation model that deals with artifacts detection and illumination bias correction inherently, within the same single variational model. To this end, we introduce a binary artifact label X, that marks individual pixels as artifacts if they violate the two-phase piece-wise constancy assumption of the CV segmentation model. We show how this approach effectively corresponds to statistical hypothesis testing; more particularly, a pixel is classified as artifact if it fails the Gaussian null-hypothesis by virtue of a $z-$score more extreme than a given threshold. This threshold parameter thus directly controls the statistical significance level associated with the artifact classification, or the expected false-positive rate, respectively. We call this the *CV+X* model. On the other hand, to deal with illumination bias, we include a Retinex-like image decomposition. Starting from a simple additive image formation model, $I = B + S$, we decompose the input image I into a structure part S and a smooth bias B. The structure part is expected to be two-phase piecewise constant, as modeled by the CV-terms. We call this second variant the *CV+B* model. Combining both parts performs image segmentation coupled with dynamic artifacts detection and bias estimation as intended. The resulting full *CV+XB* model yields as output: A binary segmentation u, the region characteristics μ_1 and μ_2, an artifact map X, a nearly two-phase structure estimate S, and a smooth bias field B. We also propose a numerical scheme to minimize this model efficiently, based on MBO-like threshold dynamics, which has proven much faster

than the gradient descent approach. In practical results included in this paper we show that the model is adept at correctly segmenting artifact and bias affected images.

The remainder of this paper is structured as follows. First, in §2 we provide some more complementary background on the CV model as relevant to our work. We then address the artifact detection (§3) and bias correction (§4) problem separately, before we put them together in a single combined variational model (§5). We present results and a discussion of our model in §6 and conclude in §7.

2. More Background on the CV Model.
In the following paragraphs, we review some aspects of and modifications to the CV model [7], both in terms of model formulation and algorithms for its optimization, that are going to guide the development of our proposed artifact- and bias-resistant segmentation model.

2.1. Gradient descent.
The original and immediate strategy to solve the CV model (3) was gradient descent. Calculus of variations yields the following iterative updates:

$$\mu_1 = \frac{\int_\Omega I \cdot H(\phi)}{\int_\Omega H(\phi)}, \quad \mu_2 = \frac{\int_\Omega I \cdot (1 - H(\phi))}{\int_\Omega (1 - H(\phi))}, \tag{4}$$

which is to say that μ_1 and μ_2 are the average colors of their respective regions, and

$$\frac{\partial \phi}{\partial t} = \delta(\phi) \left[\beta \operatorname{div} \left(\frac{\nabla \phi}{|\nabla \phi|} \right) - \lambda_1 (I - \mu_1)^2 + \lambda_2 (I - \mu_2)^2 \right]. \tag{5}$$

2.2. Heaviside approximations.
In practice, for this, the distributional Heaviside H and its derivative δ need to be smoothly approximated by analytical H_ε and $\delta_\varepsilon = H_\varepsilon'(\phi)$, such as the logistic function and its derivative. Still, the $\delta_\varepsilon(\phi)$ term in the gradient descent means that the contour ϕ cannot change except very near the zero-level set of ϕ. This makes it difficult to provide fast segmentations with changing topologies. Thus, most implementations of the Chan-Vese model use a modified descent without the Dirac-masking (equivalently, this corresponds to the ultimate Heaviside approximation $H_\varepsilon(\phi) = \phi$ and $\delta_\varepsilon(\phi) = 1$),

$$\frac{\partial \phi}{\partial t} = \left[\beta \operatorname{div} \left(\frac{\nabla \phi}{|\nabla \phi|} \right) - \lambda_1 (I - \mu_1)^2 + \lambda_2 (I - \mu_2)^2 \right], \tag{6}$$

which arises from the energy functional proposed by Chan, Esedoglu, and Nikolova [9]:

$$E_{\text{CEN}}(\mu_1, \mu_2, \phi) = \int_\Omega |\nabla \phi| + \int_\Omega \left[\lambda_1 (I - c_1)^2 - \lambda_2 (I - c_2)^2 \right] \phi. \tag{7}$$

The latter energy, however, is homogeneous of degree 1 in ϕ, and it does not have a minimizer in general. In other words, the modified gradient descent does not have a stationary state and the level set function ϕ would tend to $\pm\infty$ if the evolution was carried out for long enough time [9]. As a consequence, the level-set function is often restricted to take a particular shape, such as being a signed distance function [25, 26, 15]. Alternatively, Chan et al. [9] show that restricting the level-set function to values within the convex set $\phi \in [0, 1]$ renders the solutions of (7) to be the solutions of the original CV model (3). The level-set function in the modified model effectively represents a convex relaxation of the characteristic function $H(\phi)$ of the original CV model, and is also called phase-field. By allowing movement of the contour at all locations, this adapted model allows for faster changes in topology and therefore faster segmentation.

2.3. **Threshold dynamics for mean curvature motion.** Irrespective of the chosen Heaviside approximation H_ε, the CV-PDE (5) is hard to solve, due to the presence of the divergence term associated with the interface perimeter. This divergence term actually represents the mean curvature of the interface, i.e., if it were only up to this regularization term, then the active contour would be moving with a velocity proportional to its mean-curvature. Unfortunately, one can expect difficulties with this term, for example in flat regions where $|\nabla \phi| \to 0$, which is why some authors prefer maintaining ϕ as a signed distance function with $|\nabla \phi| = 1$ (a.e.). Moreover, if the PDE is integrated explicitly, then the time step is also heavily limited by the CFL condition [11].

An important contribution towards more efficient CV optimization stems from the phase-field approach outlined in [14], and goes back to the diffusion-threshold scheme for approximating motion by mean curvature proposed by Merriman, Bence, and Osher [29]. The fundamental idea is to reproduce the motion by mean curvature due to the divergence term in the CV-PDE (5) by more efficient means.

For this, let us replace the total variation of the phase field $u \in W^{1,2}(\Omega)$, by the real Ginzburg-Landau (also known as Allen-Cahn) functional [30] (we use the variable u instead of ϕ to highlight its phase-field nature rather than just being a generic level set function):

$$E_{\text{GL}}^\varepsilon(u) := \varepsilon \int_\Omega |\nabla u(x)|^2 dx + \frac{1}{\varepsilon} \int_\Omega W(u(x)) dx, \qquad \varepsilon > 0, \tag{8}$$

where $W(s)$ is a double well potential with two equal minima at $s = 0$ and $s = 1$, for example $W(s) := s^2(1-s)^2$. Minimizing this functional yields a phase field that is smooth and tends to be binary. In particular, it has been shown [30] that the GL-functional Γ-converges to the total variation functional of binary phase-fields $u \in \{0,1\}$ as $\varepsilon \to 0$:

$$E_{\text{GL}}^0(u) = \sigma(W) \int_\Omega |\nabla u|, \tag{9}$$

where $\sigma(W)$ is a surface tension term depending on the double well potential. The minimizing flow of this functional for $\varepsilon \to 0^+$ produces motion by mean curvature of the interface, which is exactly what one needs in the CV model minimization. However, now, the PDE associated with the GL-functional minimization is

$$\frac{\partial u}{\partial t} = 2\varepsilon \nabla^2 u - \frac{1}{\varepsilon} W'(u), \tag{10}$$

and this PDE is conveniently solved in a discrete-time two step time-splitting approach:

$$u_{n+\frac{1}{2}} = u_n + \tau \left(2\varepsilon \nabla^2 u_n\right) \tag{11}$$

$$u_{n+1} = u_{n+\frac{1}{2}} - \tau \left(\frac{1}{\varepsilon} W'(u_{n+\frac{1}{2}})\right), \tag{12}$$

where the first step is simply diffusion by the heat equation (obviously not actually propagated in such an explicit manner), and the second step is a simple ODE minimizing the double well potential. Indeed, the heat equation is much more efficiently solved based on convolution or spectral transforms [37]. The MBO-scheme [29] improves on this time-split GL-optimization in that the ODE is recognized as essentially performing thresholding. While the first step is reduced to propagation according to the standard heat equation, the second step in MBO is actual thresholding (projection onto the binary set $\{0,1\}$):

$$u_{n+\frac{1}{2}} = u_n + \tau \nabla^2 u_n \tag{13}$$

$$u_{n+1} = \begin{cases} 0 & \text{if } u_{n+\frac{1}{2}} \leq \frac{1}{2} \\ 1 & \text{if } u_{n+\frac{1}{2}} > \frac{1}{2}. \end{cases} \tag{14}$$

Note that other authors have devised time-split schemes for motion by mean curvature based on alternating TV-minimization and signed distance function redistancing [6, 2].

2.4. **CV model with threshold dynamics.** Esedoglu and Tsai [14] devise the following modified GL-based diffuse interface approximation to the CV-model:

$$E_{\text{CV}}^{\varepsilon}(\mu_1, \mu_2, u) = \varepsilon \int_{\Omega} |\nabla u|^2 + \frac{1}{\varepsilon} \int_{\Omega} W(u) + \lambda \int_{\Omega} \left[u^2(\mu_1 - I_0)^2 + (1 - u)^2(\mu_2 - I_0)^2 \right]. \quad (15)$$

This energy family differs from the original CV model (3) by the substitution of the TV-term by the GL-functional (8), and the squaring of the phase-field terms in the data fidelity expressions. The motivation behind the phase-field squaring is not immediately clear. It can be shown, however, that the sequence of energies $E_{\text{CV}}^{\varepsilon}$ Γ-converges to (3) as $\varepsilon \to 0^+$. The corresponding gradient descent equation is

$$\frac{\partial u}{\partial t} = 2\varepsilon \nabla^2 u - \frac{1}{\varepsilon} W'(u) - 2\lambda \left[u(\mu_1 - I_0)^2 + (u - 1)(\mu_2 - I_0)^2 \right], \quad (16)$$

for which Esedoglu and Tsai propose several different time splitting variants [14]. Their main scheme is to combine heat equation and data-fidelity forcing term in one step, and perform thresholding in the second step. However, the one scheme that seems most interesting in the context of the present work is a variant with an iteration over three steps, namely propagation of the image fidelity term ODE, followed by heat diffusion, and eventually thresholding. Also, we will not use the quadratic phase field terms. As with the original single CV-PDE, the region statistics μ_1 and μ_2 need to be updated regularly.

3. **Image Segmentation with Dynamic Artifact Detection.** Having spent some effort on the background of the CV model and the use of threshold dynamics for efficient optimization, it is now time to focus on the improvements we propose for artifact detection and bias correction. Let us start with dynamic artifact detection.

The main issue to be addressed in this section is the presence of outliers (individual or small groups of pixels) in images, that do not comply with the piecewise constant image model underlying the CV image segmentation. These outliers greatly affect the regions' intensity statistics μ_1 and μ_2 and may effectively lead to image segmentation failure. In some cases, artifacts may even be falsely detected as objects of interest in the image, because their presence outweighs the actual image contrast between background and object. This issue was partially addressed by [18] with the substitution of the quadratic data fidelity by the absolute fidelity term. However, this also represents a major difference in the underlying noise prior (Gaussian noise versus impulsive noise), and thus has consequences beyond dealing with artifacts. Also, in Jung et al.'s model, artifacts are not actively dealt with and they remain part of the segmentation.

3.1. **Prelude: Static Artifact Classification in Preprocessing.** Sometimes, artifacts are readily identifiable through preprocessing steps such as thresholding or other heuristics. If this is the case, then one simple approach is to eliminate the fidelity term in these regions.

Definition 3.1. We denote

$$X : \Omega \to \{0, 1\}$$

as an artifact indicator function. We accommodate this additional information in the CV model by using X as a mask on the data-fidelity term:

$$E_{\text{CVX}}^{\text{static}}(\mu_1, \mu_2, \phi) = \lambda_1 \int_{\Omega} (1 - X)(\mu_1 - I_0)^2 H(\phi) + \lambda_2 \int_{\Omega} (1 - X)(\mu_2 - I_0)^2 (1 - H(\phi))$$

$$+ \beta \int_{\Omega} |\nabla H(\phi)|, \quad (17)$$

where $(1-X) = 1$ in regions classified as non-artifacts.

Remark 1. It is important to note that the perimeter term is *not* affected by the artifact classification, and interface regularization will exclusively drive the contour evolution in regions classified as artifacts. The net effect of the introduction of X is to inhibit the data-fidelity term locally in regions that are not believed to comply with the two-phase piecewise constant image model in the first place.

This is illustrated by the (idealized) gradient descent equations:

$$\frac{\partial \phi}{\partial t} = \delta(\phi) \left[\beta \operatorname{div} \left(\frac{\nabla \phi}{|\nabla \phi|} \right) - \lambda_1 (1-X)(I-\mu_1)^2 + \lambda_2 (1-X)(I-\mu_2)^2 \right] \tag{18}$$

for μ_1, μ_2 fixed. These region statistics in turn are determined as

$$\mu_1 = \frac{\int_\Omega (1-X) \cdot I \cdot H(\phi)}{\int_\Omega (1-X) \cdot H(\phi)}, \quad \mu_2 = \frac{\int_\Omega (1-X) \cdot I \cdot (1-H(\phi))}{\int_\Omega (1-X) \cdot (1-H(\phi))}, \tag{19}$$

i.e., the computation of the mean intensity is restricted to regions not being artifacts, and provided that these regions are actually non-empty:

$$\int_\Omega (1-X) \cdot (1-H(\phi)) \neq 0 \neq \int_\Omega (1-X) \cdot H(\phi). \tag{20}$$

3.2. **Dynamic Artifact Classification.** Being able to work with artifact classification from preprocessing and partially excluding these regions from the segmentation process is one thing. It would be much more elegant, however, if preprocessing could be avoided and the artifact detection were integrated into the very same variational model. This is the goal of this section.

While in some specific applications artifacts may follow known statistical distributions in terms of shape, location, size or appearance, in the general case this is not true. Instead, here we describe artifacts by exclusion, *only knowing what they are not*. Indeed, we may characterize artifacts as isolated or small groups of pixels that fail to adhere to the two-phase piecewise constant image model, without any other prior regarding their intensity distribution or artifact shape regularity.

Definition 3.2. To this end, we simply add a penalty γ on the size of the artifact class, and optimize for X along with the actual segmentation. The CV image segmentation with dynamic artifact labeling model is defined as follows:

$$E_{\text{CVX}}(\mu_1, \mu_2, \phi, X) = \lambda_1 \int_\Omega (1-X)(\mu_1 - I_0)^2 H(\phi) + \lambda_2 \int_\Omega (1-X)(\mu_2 - I_0)^2 (1-H(\phi))$$
$$+ \beta \int_\Omega |\nabla H(\phi)| + \gamma \int_\Omega X. \tag{21}$$

The preliminary interpretation is that now the artifact indicator function X optimizes a trade-off between size penalty γ and outlier elimination. This will become much clearer once we look at the actual minimization scheme, next.

Remark 2. In support of this model, it is important to note that similar approaches are employed in other imaging tasks: in image sequences, Ayvaci, Raptis, and Soatto [1] identify pixels overly violating the optical flow constraint as occlusions, while Yan [41] localizes individual damaged pixels for impulse-noise image in-painting.

3.3. **Minimization using gradient descent.** For the sake of analysis, we now consider the naive minimization of the proposed CV model including dynamic artifact labeling through classical alternate direction gradient descent.

Problem. *We consider the problem*

$$\min_{\mu_1,\mu_2\in\mathbb{R},\,\phi\colon\Omega\to\mathbb{R},\,X\colon\Omega\to\{0,1\}} E_{CVX}(\mu_1,\mu_2,\phi,X). \tag{22}$$

The gradient descent equations of this minimization problem with respect to the CV variables μ_1, μ_2, and ϕ are identical to the ones derived from the static functional (17), and have been given in (18) and (19). In addition, now, at each iteration of coordinate descent, we need the optimal update of the artifact indicator X.

Lemma 3.3. *At each iteration, the artifact indicator function X needs to satisfy*

$$X^* := \underset{X\colon\Omega\to\{0,1\}}{\arg\min} E_{CVX}(\mu_1,\mu_2,\phi,X). \tag{23}$$

This update is locally found as

$$X^*(x) = \begin{cases} 0 & if \quad \lambda_1(\mu_1 - I_0)^2 H(\phi) + \lambda_2(\mu_2 - I_0)^2(1 - H(\phi)) \leq \gamma \\ 1 & otherwise \end{cases} \quad x \in \Omega. \tag{24}$$

Proof. The local cost associated with X is

$$c(x) := (1 - X)\cdot\left[\lambda_1(\mu_1 - I_0)^2 H(\phi) + \lambda_2(\mu_2 - I_0)^2(1 - H(\phi))\right] + X\cdot\gamma \quad x \in \Omega, \tag{25}$$

and the optimal X^* satisfies

$$X^*(x) = \underset{X(x)\in\{0,1\}}{\arg\min} c(x), \quad \forall x \in \Omega. \tag{26}$$

Since $X \in \{0,1\}$ locally, there are only two cases to be considered at each pixel:

$$c(x) = \begin{cases} \lambda_1(\mu_1 - I_0)^2 H(\phi) + \lambda_2(\mu_2 - I_0)^2(1 - H(\phi)) & \text{if} \quad X(x) = 0 \\ \gamma & \text{if} \quad X(x) = 1, \end{cases} \quad x \in \Omega. \tag{27}$$

The optimizer X^* simply picks the lesser cost between those two cases, locally for each pixel. $\qquad\square$

Remark 3. We include this proof despite being trivial, because it highlights the impact of the artifact indicator X. Indeed, let us assume that the parameters λ_1 and λ_2 represent the inverse of the Gaussian noise variance from a Bayesian interpretation of the CV model [4]. Without loss of generality, consider now a pixel x in the object region, $H(\phi(x)) = 1$. The relevant term in (24) is thus

$$\lambda_1(\mu_1 - I_0)^2 \propto \left(\frac{I_0 - \mu_1}{\sigma}\right)^2,$$

which is the squared z-score (standard score) of the local intensity under a Gaussian distribution of corresponding region statistics. This squared z-score is then compared against the threshold γ. The immediate interpretation is thus the following: the artifact classification is effectively a concealed statistical hypothesis *z*-test of the pixel intensity with a Gaussian distribution $\mathcal{N}(\mu_i,\lambda_i)$ as null-hypothesis, and a pixel is classified as an artifact if the *z*-score of its intensity is more extreme than $\sqrt{\gamma}$. The model parameter γ is thus intimately related to the level of statistical significance attached to the artifact classification and its expected false positives rate.

3.4. **Minimization using threshold dynamics.** Let us now make use of the phase-field approach and threshold dynamics to propose a more efficient optimization scheme for the CV+X problem.

Definition 3.4. First, we replace the levelset function ϕ, respectively its Heaviside term, $H(\phi)$, by the phase-field $u\colon \Omega \to [0,1]$. We thus rewrite the CV+X model (21) as follows:

$$E_{\text{CVX}}(\mu_1,\mu_2,u,X) = \lambda_1 \int_\Omega (1-X)(\mu_1 - I_0)^2 u + \lambda_2 \int_\Omega (1-X)(\mu_2 - I_0)^2 (1-u)$$
$$+ \beta \int_\Omega |\nabla u| + \gamma \int_\Omega X. \quad (28)$$

Problem. *The resulting image segmentation with dynamic artifact classification problem thus becomes*

$$\min_{\mu_1,\mu_2\in\mathbb{R},\, u\colon \Omega\to[0,1],\, X\colon \Omega\to\{0,1\}} E_{CVX}(\mu_1,\mu_2,u,X). \quad (29)$$

Due to the newly introduced artifact variable X modulating the data-fidelity term, the resulting energy functional is non-convex and the global minimizer results from [9] do not fully apply to the associated minimization problem. We propose solving the minimization problem in a coordinate descent approach. Starting from some suitable initialization u^0, and $X^0 = 0$, iterate

$$\mu_1^{n+1},\mu_2^{n+1} \leftarrow \operatorname*{arg\,min}_{\mu_1,\mu_2\in\mathbb{R}} E_{\text{CVX}}(\mu_1,\mu_2,u^n,X^n) \quad (30)$$

$$u^{n+1} \leftarrow \operatorname*{arg\,min}_{u\colon \Omega\to[0,1]} E_{\text{CVX}}(\mu_1^{n+1},\mu_2^{n+1},u,X^n) \quad (31)$$

$$X^{n+1} \leftarrow \operatorname*{arg\,min}_{X\colon \Omega\to\{0,1\}} E_{\text{CVX}}(\mu_1^{n+1},\mu_2^{n+1},u^{n+1},X) \quad (32)$$

until convergence, and *hope* that the sequence $(\mu_1^n,\mu_2^n,u^n,X^n)$ of subminimizers thusly obtained converge to the true minimizer of the problem,

$$\lim_{n\to\infty}(\mu_1^n,\mu_2^n,u^n,X^n) = \operatorname*{arg\,min}_{\mu_1,\mu_2\in\mathbb{R},\, u\colon \Omega\to[0,1],\, X\colon \Omega\to\{0,1\}} E_{\text{CVX}}(\mu_1,\mu_2,u,X).$$

The idea behind our proposed minimization scheme is to combine the threshold dynamics of Esedoglu and Tsai's [14] CV-model with the artifact detection part outlined above. To this end, we perform time-splitting on the gradient descent scheme w.r.t. the phase-field, to separate the data-fidelity ODE from the heat-diffusion PDE, followed by thresholding, and update the region statistics μ_1 and μ_2, and the artifact classification as before.

Algorithm 1. *The phase-field CV+X energy* (28) *can be efficiently minimized, and thus problem* (29) *(image segmentation with dynamic artifact classification) be solved, by repeating the following steps until convergence, for some appropriate time-step $\tau > 0$:*

1. *Update μ_1 and μ_2 using* (19),
2. *Evolve phase-field u for some time τ each (possibly several times):*
   (a) According to the data term including the artifact mask,

$$\frac{\partial u}{\partial t} = (1-X)\left[-\lambda_1(I-\mu_1)^2 + \lambda_2(I-\mu_2)^2\right]$$

   (b) According to the heat equation

$$\frac{\partial u}{\partial t} = \nabla^2 u$$

   with the updated phase-field as initial condition and using appropriate boundary conditions, (e.g. Neumann or periodic),

(c) Update u by thresholding:

$$u = \begin{cases} 1 & \textit{if} \quad u > \frac{1}{2} \\ 0 & \textit{otherwise} \end{cases}$$

3. Update X as in (24).

The algorithm will be empirically corroborated by diverse practical results, in §6 below.

4. **Image Segmentation with Bias Correction.** Let us now entirely switch gears and focus not on the artifacts, but inhomogeneous illumination affecting the image to be segmented. The consequence of inhomogeneous illumination is that the same *material* (object or background) does not have a *uniform appearance* over the entire image domain. More specifically, the image pixels of a region of interest are not all drawn from the same idealized Gaussian distribution, since the mean intensity of such a region varies across Ω due to inhomogeneous illumination, and a region cannot be characterized by its mean intensity and noise variance anymore. More abstractly, the very two-phase piecewise constancy assumption of the Chan-Vese [7] cartoon limit to the Mumford-Shah [32] model is violated. One way to deal with this complication is to abandon the CV assumptions partially, and to model images to be segmented as piecewise smooth, instead. This path was chosen by Li, Kao, Gore and Ding, with their popular region-scalable fitting energy for image segmentation [24]. Here, we want to maintain the piecewise constancy assumption of the CV model, and deal with the illumination inhomogeneity by decomposing the image into its (piecewise constant) structure and an (illumination) bias part.

4.1. **Retinex assumption.** Retinex is a theory on the human visual perception [21, 22, 23]. It was an attempt at explaining how a combination of processes supposedly taking place both in the retina and the cortex is capable of adaptively coping with illumination that varies spatially [43, 44]. The fundamental observation is the insensitivity of human visual perception with respect to a slowly varying illumination on a Mondrian-like piecewise constant scene.

Starting from an additive image formation model[2],

$$i(x) = b(x) + s(x), \tag{33}$$

where the illumination b is supposed to vary smoothly, the spatial derivatives of the observed intensity i are mostly due to edges in the structure s. This is the core assumption to most Retinex implementations, such as [17, 20, 31]. Here, we propose to integrate this Retinex model into the CV image segmentation model, by considering only the piecewise constant image part, and discarding the smoothly varying illumination bias.

4.2. **Prelude: Static Bias Field Correction in Preprocessing.** The most immediate solution might consist in performing Retinex image decomposition as a preprocessing step to CV image segmentation. Indeed, one can pick his most favorite Retinex algorithm to split the image to be segmented into a smooth bias field and a piecewise constant structure part, for example [28], and then run the CV model on only the extracted structure part. This could be an unwise strategy, however, since the CV image model is not just expecting a piecewise constant input image, but more specifically a *two-phase* piecewise constant image, which is a much stronger image prior, simply ignored in such Retinex preprocessing.

---

[2]Such an additive model can be derived from the common multiplicative image formation model $I(x) = B(x)S(x)$, where I is the observed intensity, B is illumination bias and S is reflectance, by taking the logarithm, $i := \log(I)$ etc.

4.3. **Dynamic Bias Field Correction.** Instead, we propose to integrate the Retinex image decomposition and the CV image segmentation problem into a single variational model: We are interested in an image decomposition consisting of a smooth bias field and a two-phase piecewise constant structure part with regular phase interface. In this, rather than segment an image directly, the model seeks to segment the image's underlying structure. Instead of extracting this structure via preprocessing, however, we optimize segmentation and bias correction simultaneously.

Definition 4.1. Let

$$B, S \colon \Omega \to \mathbb{R}$$

denote the estimated bias and structure part, respectively. Then, we define the energy functional for joint image segmentation and bias correction as follows (in original CV-like notation):

$$E_{\mathrm{CVB}}(\mu_1, \mu_2, \phi, B, S) := \lambda_1 \int_\Omega (\mu_1 - S)^2 H(\phi) + \lambda_2 \int_\Omega (\mu_2 - S)^2 (1 - H(\phi))$$
$$+ \beta \int_\Omega |\nabla H(\phi)| + \alpha \int_\Omega |\nabla B|^2, \quad (34)$$

where the first three terms are the classical CV model acting on the structure S instead of the input image I_0, while the new term models bias smoothness.

Remark 4. Note that the proposed model (34) differs from a simple two-phase approximation of the MS-functional (1) in that the bias field, B, representing the smooth variations, is restricted to be smooth *everywhere*, thus in particular at the phase interface.

Problem. *Performing joint image decomposition and segmentation based on the functional* (34) *thus amounts to solving the following constraint minimization problem:*

$$\min_{\mu_1, \mu_2 \in \mathbb{R}, \, \phi, B, S \colon \, \Omega \to \mathbb{R}} E_{CVB}(\mu_1, \mu_2, \phi, B, S) \qquad s.t. \quad I_0 = B + S, \qquad (35)$$

where the constraint represents the image formation model (33).

4.4. **Minimization.** As for the original CV model (3) or the CV+X model (21), the proposed functional (34) can be reformulated in phase-field terms, replacing $H(\phi)$ by $u \colon \Omega \to [0, 1]$. The resulting minimization scheme is then analogous to the previous schemes as regards the optimization of μ_1, μ_2, and u. The interesting part of the problem, namely, the newly arising minimization with respect to the structure-bias decomposition, however, is independent of the chosen domain parameterization (levelset vs. phase-field). Instead, an interesting issue is related to the image formation constraint $I_0 = B + S$.

Indeed, this linear constraint can be softly enforced by simply adding a quadratic penalty term

$$\rho \int_\Omega |I_0 - B - S|^2,$$

and then solving the resulting unconstrained minimization problem (the *Penalty method*). Strictly enforcing the image formation model using this penalty, only, would require $\rho \to \infty$, which renders the functional ill-conditioned. If the constraint is to be imposed strictly, in addition to the quadratic penalty term, a Lagrangian multiplier can be employed while keeping ρ finite [33] (the *Augmented Lagrangian* method).

Definition 4.2. Let us do so and define the Augmented Lagrangian corresponding to the functional (34) including the image formation constraint (33), in terms of the phase-field

$u \colon \Omega \to [0,1]$, this time:

$$AL_{\mathrm{CVB}}(\mu_1, \mu_2, u, B, S, \lambda) := \lambda_1 \int_\Omega (\mu_1 - S)^2 u + \lambda_2 \int_\Omega (\mu_2 - S)^2 (1 - u) + \beta \int_\Omega |\nabla u|$$
$$+ \alpha \int_\Omega |\nabla B|^2 + \rho \int_\Omega |I_0 - B - S|^2 + \langle \lambda, I_0 - B - S \rangle_\Omega, \quad (36)$$

where λ is the newly introduced Lagrangian multiplier and $\langle \cdot, \cdot \rangle_\Omega$ denotes the standard inner product over the domain Ω.

Problem. *Solving the constrained minimization problem* (35) *can now be substituted by finding a saddle point of the Augmented Lagrangian* (36)*:*

$$\max_{\lambda \colon \Omega \to \mathbb{R}} \quad \min_{\mu_1, \mu_2 \in \mathbb{R}, \, u \colon \Omega \to [0,1], \, B,S \colon \Omega \to \mathbb{R}} \quad AL_{CVB}(\mu_1, \mu_2, u, B, S, \lambda). \quad (37)$$

This min-max problem can be solved in a coordinate descent/dual ascent approach. The subminimizations w.r.t. μ_1, μ_2, and u are analogous to what we have seen earlier, and are left as a simple exercise to the reader. We will instead focus on the new elements B, S, and the dual λ.

Lemma 4.3. *The Euler-Lagrange equation associated with the subminimization problem*

$$B^* = \underset{B \colon \Omega \to \mathbb{R}}{\arg\min} \quad AL_{CVB}(\mu_1, \mu_2, u, B, S, \lambda)$$

reads

$$-\alpha \nabla^2 B^* = \rho(I_0 - B^* - S) + \frac{\lambda}{2}, \quad (38)$$

which is simply the heat equation that can be efficiently solved, e.g., spectrally using the Fourier transform $\mathcal{F}\{\cdot\}(\omega)$ *(thus implicitly assuming periodic boundary conditions):*

$$B^* = \mathcal{F}^{-1} \left\{ \frac{\mathcal{F}\left\{\rho(I_0 - S) + \frac{\lambda}{2}\right\}(\omega)}{\rho + \alpha|\omega|^2} \right\}. \quad (39)$$

Proof. These EL-equations directly result from simple calculus of variations on the three relevant terms of (36) involving B. This first variation reads

$$\partial_B AL_{\mathrm{CVB}} = -2\alpha \nabla^2 B - 2\rho(I_0 - B - S) - \lambda, \quad (40)$$

and using the optimality condition $\partial_B AL_{\mathrm{CVB}} = 0$, the EL equations (38) are immediately obtained. $\qquad\square$

Remark 5. The immediate interpretation of the B-update is as follows: B strives to optimize the trade-off between image formation constraint $I_0 - S$ and the smoothness prior imposed by $|\nabla B|^2$, and B is updated as a lowpass filtered version of what $I_0 - S$ suggests. As will be seen farther below, the Lagrangian multiplier λ accumulates the error on the reconstruction constraint, and will eventually enforce that constraint strictly.

Similarly, let us now determine the EL-equations governing the update of the structure image S:

Lemma 4.4. *The Euler-Lagrange equation associated with the subminimization problem*

$$S^* = \underset{S \colon \Omega \to \mathbb{R}}{\arg\min} \quad AL_{CVB}(\mu_1, \mu_2, u, B, S, \lambda)$$

reads

$$S^* = \frac{\lambda_1 \mu_1 u + \lambda_2 \mu_2 (1 - u) + \rho(I_0 - B) + \frac{\lambda}{2}}{\lambda_1 u + \lambda_2 (1 - u) + \rho} \qquad \forall x \in \Omega. \quad (41)$$

Proof. The EL equation (41) is immediately obtained by computing the first variation of the Augmented Lagrangian (36) along S,

$$\partial_S AL_{\text{CVB}} = -2\lambda_1(\mu_1 - S)u - 2\lambda_2(\mu_2 - S)(1 - u) - 2\rho(I_0 - B - S) - \lambda, \qquad (42)$$

and using the optimality condition $\partial_S AL_{\text{CVB}} = 0$. $\qquad\square$

Remark 6. This update for the structure variable S again admits an immediate and intuitive interpretation: S balances the trade-off between the image decomposition rule $I - B$ and compliance with the piecewise constancy terms due to the CV model, achieved by averaging the two contributions. Again, the error-accumulating Lagrangian multiplier adds the error back into the updates.

Finally, we note that the Lagrangian multiplier is simply updated through gradient ascent (dual ascent), through propagation of the following ODE

$$\frac{\partial \lambda}{\partial t} = \partial_\lambda AL_{\text{CVB}} = I_0 - B - S, \qquad (43)$$

from which the error-accumulating nature of the Lagrangian multiplier becomes evident.

We summarize our proposed optimization algorithm for the CV+B image segmentation with bias correction model, based on the phase-field approximation:

Algorithm 2. *The joint image segmentation and bias correction problem can be solved by minimizing the constrained CV+B energy (34), through its surrogate, the associated Augmented Lagrangian saddle point problem (37). To this end, starting from some initialization u^0, and $S^0 = I_0$, $B^0 = 0$[3], we repeat the following steps until convergence, for some appropriate time-step $\tau > 0$:*

1. *Update μ_1 and μ_2 using (4), substituting S for I*
2. *Evolve the phase-field u for some time τ each (possibly several times):*
   (a) According to the CV-data term on the structure part,

$$\frac{\partial u}{\partial t} = \left[-\lambda_1(S - \mu_1)^2 + \lambda_2(S - \mu_2)^2 \right]$$

   (b) According to the heat equation

$$\frac{\partial u}{\partial t} = \nabla^2 u$$

   with the previously updated phase-field as initial condition and using appropriate boundary conditions
   (c) Rectify the diffused u by thresholding:

$$u = \begin{cases} 1 & if \quad u > \frac{1}{2} \\ 0 & otherwise \end{cases}$$

3. *Update the bias field estimate B spectrally according to (39)*
4. *Update the structure estimate S according to (41)*
5. *Update the Lagrangian multiplier λ by dual ascent (43).*

Again, the algorithm is supported by positive practical results, as will be shown later in this work (§6).

---

[3]A smarter initialization of the structure-bias-decomposition can be based on a Retinex-preprocessing step.

5. **Combined Artifact Detection and Bias Corrective Image Segmentation Model.** Having tuned the original CV model to deal with artifact or illumination bias corrupted images, respectively, we have now all ingredients ready to build a single variational, region-based image segmentation model that inherently detects local artifacts and corrects smoothly varying illumination bias. Having both components is crucial, because either type of corruption has the critical potential to prevent correctly handling the other. On the one hand, artifacts and outliers can exert a great negative impact on most Retinex decomposition models, since their resulting high contrast cannot be accommodated in the bias field but would need to be attributed to the structure, distorting the intensity information even outside the actual artifact regions. Uneven illumination, on the other hand, has the potential to identify artifacts falsely if it pushes the intensities of some pixels outside their respective region's "comfort zone" in terms of distance from the mean intensity. Having artifact and bias terms in a single variational functional allows handling of these complications concurrently.

5.1. **Combined model.** Formulating this single variational model involving both dynamic artifact detection and bias correction is now merely a matter of combining the respective definitions of CV+X (21) and CV+B (34):

Definition 5.1. Let $X\colon \Omega \to \{0,1\}$ denote the artifact indicator function, and let $B, S\colon \Omega \to \mathbb{R}$ be the bias and structure decomposition of the input image $I_0\colon \Omega \to \mathbb{R}$. We define the CV+XB functional for *joint image segmentation, artifact classification, and bias correction* as the following energy.

$$E_{\text{CVXB}}(\mu_1, \mu_2, \phi, X, B, S) := \lambda_1 \int_\Omega (1-X)(\mu_1-S)^2 H(\phi)$$
$$+ \lambda_2 \int_\Omega (1-X)(\mu_2-S)^2 (1-H(\phi)) + \beta \int_\Omega |\nabla H(\phi)| + \gamma \int_\Omega X + \alpha \int_\Omega |\nabla B|^2, \quad (44)$$

or, for purposes of more efficient optimization, in terms of the phase-field approximation $H(\phi) \approx u\colon \Omega \to [0,1]$:

$$E_{\text{CVXB}}(\mu_1, \mu_2, u, X, B, S) := \lambda_1 \int_\Omega (1-X)(\mu_1-S)^2 u + \lambda_2 \int_\Omega (1-X)(\mu_2-S)^2 (1-u)$$
$$+ \beta \int_\Omega |\nabla u| + \gamma \int_\Omega X + \alpha \int_\Omega |\nabla B|^2. \quad (45)$$

Remark 7. It is important to note that in this combined model, the artifact variable X only masks the CV terms on the structure part S, while interface perimeter $TV(u)$ and bias field smoothness $|\nabla B|^2$ are not affected.

Problem. *To perform joint image segmentation, artifact classification and bias correction we now propose to solve the following constrained minimization problem (here in terms of the phase-field u already):*

$$\min_{\mu_1, \mu_2 \in \mathbb{R},\, u\colon \Omega \to [0,1],\, X\colon \Omega \to \{0,1\},\, B,S\colon \Omega \to \mathbb{R}} E_{CVXB}(\mu_1, \mu_2, u, X, B, S) \qquad s.t. \quad I_0 = B + S,$$
$$(46)$$

5.2. **Minimization.** Like in the CV+B case, one feasible way of solving this constraint minimization problem is to incorporate the image formation model constraint as both a quadratic penalty and a Lagrangian multiplier to form an Augmented Lagrangian, and then to proceed by solving the associated (unconstrained) saddle point problem.

Definition 5.2. To this end, we introduce the Augmented Lagrangian for the CV+XB min-imization problem (46), based on its phase-field functional (45):

$$AL_{\mathrm{CVXB}}(\mu_1,\mu_2,u,X,B,S) := \lambda_1 \int_\Omega (1-X)(\mu_1-S)^2 u + \lambda_2 \int_\Omega (1-X)(\mu_2-S)^2(1-u)$$

$$+ \beta \int_\Omega |\nabla u| + \gamma \int_\Omega X + \alpha \int_\Omega |\nabla B|^2 + \rho \int_\Omega |I_0 - B - S|^2 + \langle \lambda, I_0 - B - S \rangle_\Omega, \quad (47)$$

where $\lambda \colon \Omega \to \mathbb{R}$ is the Lagrangian multiplier.

Problem. *The constrained minimization problem* (46) *can now be substituted by the saddle point problem of the Augmented Lagrangian* (47)*:*

$$\max_{\lambda \colon \Omega \to \mathbb{R}} \quad \min_{\mu_1,\mu_2 \in \mathbb{R},\, u \colon \Omega \to [0,1],\, X \colon \Omega \to \{0,1\},\, B,S \colon \Omega \to \mathbb{R}} \quad AL_{CVXB}(\mu_1,\mu_2,u,X,B,S,\lambda). \quad (48)$$

In the usual way, this saddle point problem is solved by coordinate descent and dual ascent. All of the relevant subminimization problems have been discussed so far, and only slight modifications are needed here; the subminimization problems w.r.t. *S*, *X* and μ_1,μ_2 are the only ones affected by an overlap of terms stemming from the artifact detection and the bias correction model. Indeed, the CV terms include both the structure *S* and the mask *X*, as well as the statistics, which impacts their respective subminimization problems as follows:

1. The statistics are now updated based on the masked, estimated structure *S*.
2. The artifacts are detected based on the structure, rather than the original input image.
3. Finally, where no artifacts are detected the structure update is a tradeoff between image formation model and CV two-phase piecewise constancy (as before); in the presence of artifacts, however, the structure is exclusively derived from the image formation model.

The Euler-Lagrange equation for the structure update

$$S^* = \underset{S \colon \Omega \to \mathbb{R}}{\arg\min} \quad AL_{\mathrm{CVXB}}(\mu_1,\mu_2,u,X,B,S,\lambda)$$

is indeed found as

$$S^* = \frac{(1-X)\left[\lambda_1\mu_1 u + \lambda_2\mu_2(1-u)\right] + \rho(I_0-B) + \frac{\lambda}{2}}{(1-X)\left[\lambda_1 u + \lambda_2(1-u)\right] + \rho} \qquad \forall x \in \Omega. \quad (49)$$

Putting all previous results and their adaptations together as described, we propose the following algorithm for the CV+XB model:

Algorithm 3. *The joint image segmentation, artifact detection, and bias correction problem can be solved by minimizing the constrained CV+XB energy* (44)*, viz. by solving the associated Augmented Lagrangian saddle point problem* (48)*. Starting from some initialization u^0, $X^0 = 0$, $S^0 = I_0$, and $B^0 = 0$, we iterate these steps until convergence, for some appropriate time-step $\tau_u, \tau_\lambda > 0$:*

1. *Update μ_1 and μ_2 using*

$$\mu_1^{n+1} = \frac{\int_\Omega (1-X) \cdot S \cdot H(\phi)}{\int_\Omega (1-X) \cdot H(\phi)}, \quad \mu_2^{n+1} = \frac{\int_\Omega (1-X) \cdot S \cdot (1-H(\phi))}{\int_\Omega (1-X) \cdot (1-H(\phi))},$$

2. *Evolve the phase-field u for some time τ_u each (possibly several times):*
   (a) *According to the CV-data term on the structure part,*

$$\frac{\partial v}{\partial t} = (1-X) \cdot \left[-\lambda_1 (S-\mu_1)^2 + \lambda_2 (S-\mu_2)^2 \right],$$

   with $v(x,0) = u^n(x)$ as initial condition,

(b) *According to the heat equation*

$$\frac{\partial w}{\partial t} = \nabla^2 w,$$

with the previously propagated phase-field $w(x,0) = v(x,\tau_u)$ as initial condition and using appropriate boundary conditions,

(c) *Rectify the diffused w by thresholding:*

$$u^{n+1}(x) = \begin{cases} 1 & if \quad w(x,\tau_u) > \frac{1}{2} \\ 0 & otherwise, \end{cases} \qquad x \in \Omega,$$

3. *Update the artifact classification X according to*

$$X^{n+1}(x) = \begin{cases} 0 & if \quad \lambda_1(\mu_1 - S)^2 u + \lambda_2(\mu_2 - S)^2(1-u) \leq \gamma \\ 1 & otherwise, \end{cases} \qquad x \in \Omega,$$

4. *Update the bias field estimate B spectrally according to* (39)*:*

$$B^{n+1} = \mathcal{F}^{-1}\left\{ \frac{\mathcal{F}\left\{\rho(I_0 - S) + \frac{\lambda}{2}\right\}(\omega)}{\rho + \alpha|\omega|^2} \right\},$$

5. *Update the structure estimate S pointwise according to* (49)

$$S^{n+1} = \frac{(1-X)[\lambda_1\mu_1 u + \lambda_2\mu_2(1-u)] + \rho(I_0 - B) + \frac{\lambda}{2}}{(1-X)[\lambda_1 u + \lambda_2(1-u)] + \rho}, \qquad \forall x \in \Omega,$$

6. *Update the Lagrangian multiplier λ by dual ascent* (43)*,*

$$\lambda^{n+1} = \lambda^n + \tau_\lambda(I_0 - B - S).$$

Practical results obtained with this algorithm are presented in §6, next.

6. **Results and Discussion.** We have implemented the complete CV+XB model according to the algorithm outlined in algorithm 3 of §5.2, in MATLAB[4]. This full model includes the sub-models CV, CV+X, and CV+B, easily selected by simply suppressing some or all of the sub-updates to X, S, and B listed in algorithm 3.

First, we use test images provided[5] by the authors of the region-scalable fitting model [24]. These five images mainly illustrate the use of bias field estimation incorporated into the segmentation problem. In addition, for a specific case for the artifact detection model, we test our model on a synthetic test image of ellipses[6].

All six test images have been processed with all four models, and the results are illustrated in figures 1-3. Images and results are described in detail in the figure captions. Slight tuning of model parameters was necessary between images (but not between models for a single image). This is natural since images greatly vary in noise level, bias smoothness, outlier presence, etc. The success of the segmentation models depends on the chosen model and image considered; naturally, not all of the images are equally affected by bias and artifacts, and only appropriate priors and model choices fit. Most images worked impressively well, and the algorithm converged rapidly, typically within 10 and 50 iterations, amounting to fractions of a second on standard personal computing equipment (2011 laptop with Intel Core i7 2.80 GHz (dual core), 4GB RAM, running 64-bit Fedora 20 Linux OS, and MATLAB 2011b), as reported in table 1.

---

[4]code available at http://www.math.ucla.edu/~zosso/code.html and at MATLAB Central
[5]http://www.engr.uconn.edu/~cmli/code/RSF_v0_v0.1.zip
[6]found at http://www.cs.rug.nl/svcg/Shapes/Inpainting

TABLE 1. Algorithm convergence: number of iterations and required computer time. The algorithm is deterministic. Convergence is defined as the phase-field u not changing during its update. Computation time is statistical depending on CPU scheduling; here, we report average numbers over 50 repetitions. The extra cost of artifact is negligible compared to basic CV, in particular since it may speed up convergence in appropriate images. Bias correction roughly doubles the computational load per iteration, which is an acceptable price for its benefits when appropriate.

I	$M \times N$	CV		CV+X		CV+B		CV+XB	
		i [1]	t [s]	i [1]	t [s]	i [1]	t [s]	i [1]	t [s]
1	78×119	11	0.02	20	0.03	11	0.04	11	0.05
2	75×79	14	0.02	16	0.02	64	0.24	69	0.27
3	96×127	22	0.06	45	0.12	51	0.30	53	0.31
4	110×111	13	0.03	26	0.07	38	0.22	57	0.33
5	131×103	33	0.11	33	0.12	27	0.23	27	0.25
6	124×184	11	0.05	18	0.07	41	0.32	23	0.19

We further apply the proposed models to real images from atomic force microscopy (AFM) and fluorescence microscopy. In figures 4 and 5 we present both the classical CV result as well as the most appropriate proposed model for each case (CV+X, CV+B, or CV+XB). In all these images, our models allow significant improvement of the segmentation, while also providing additional information about artifact location and/or structure-bias decomposition, where applicable. For scientific use of these segmentations see [38].

7. **Conclusions.** In this paper, we have presented an energy functional that describes joint region-based image segmentation, dynamic artifact classification, and bias field estimation. Combining these tasks within a single functional allows simultaneous solution of the different problem aspects in a common variational approach, as opposed to more error-prone sequential processing. Indeed, joint optimization enables making full use of the few priors employed in the model, while sequential processing would each time focus on subsets of priors, only.

We show relations between the proposed model and state-of-the-art techniques in image processing: the proposed artifact handling is related to recent results in occlusion detection in optical flow modeling [1] and outlier handling for impulse-noise denoising [41]. In our case, we can make an elegant connection between the artifact classification performed by our model and statistical hypothesis testing: the model classifies pixels as artifacts if their $z-$score under a Gaussian noise model is more extreme than the parameter γ, which means that we have direct control over the expected error rate on artifact labeling. The bias field estimation, on the other hand, is intimately tied to the Retinex model for image decomposition. However, using a joint model, our decomposition makes direct use of the two-phase piecewise constancy assumption of the CV-model, which is a much stronger prior on the structure part than typical Retinex models employ.

In addition to formulating a joint model for these tasks, we also devise an efficient algorithm for the optimization of the proposed variational problem. Our algorithm makes use of the phase-field parameterization and threshold-dynamics [29] that have successfully been introduced to the CV-model in [9]. The algorithm solves the saddle-point problem

FIGURE 1. Example cases 1 & 2. **Top:** Coronal MRI slice. Input image and initial segmentation contour are shown in the top-right corner. The image is heavily affected by intensity bias, such that the classical CV model fails. The superior parts of the white-matter are undersegmented, while the inferior regions are markedly oversegmented. CV+X is not very helpful, here. In contrast, CV+B fixes the problem: the extracted structure is nearly flat (the brain is essentially two-phase piecewise constant), while CV+XB marks some non-brain pixels as outliers. **Bottom:** This synthethic image is a combination of piecewise constant regions affected by strong noise and oscillating bias. Again, CV fails, and artifacts detection not appropriate. Bias correction greatly improves the segmentation, but errors persist since from the simple initialization the algorithm converges to a wrong local minimum (upper part of left hand structure).

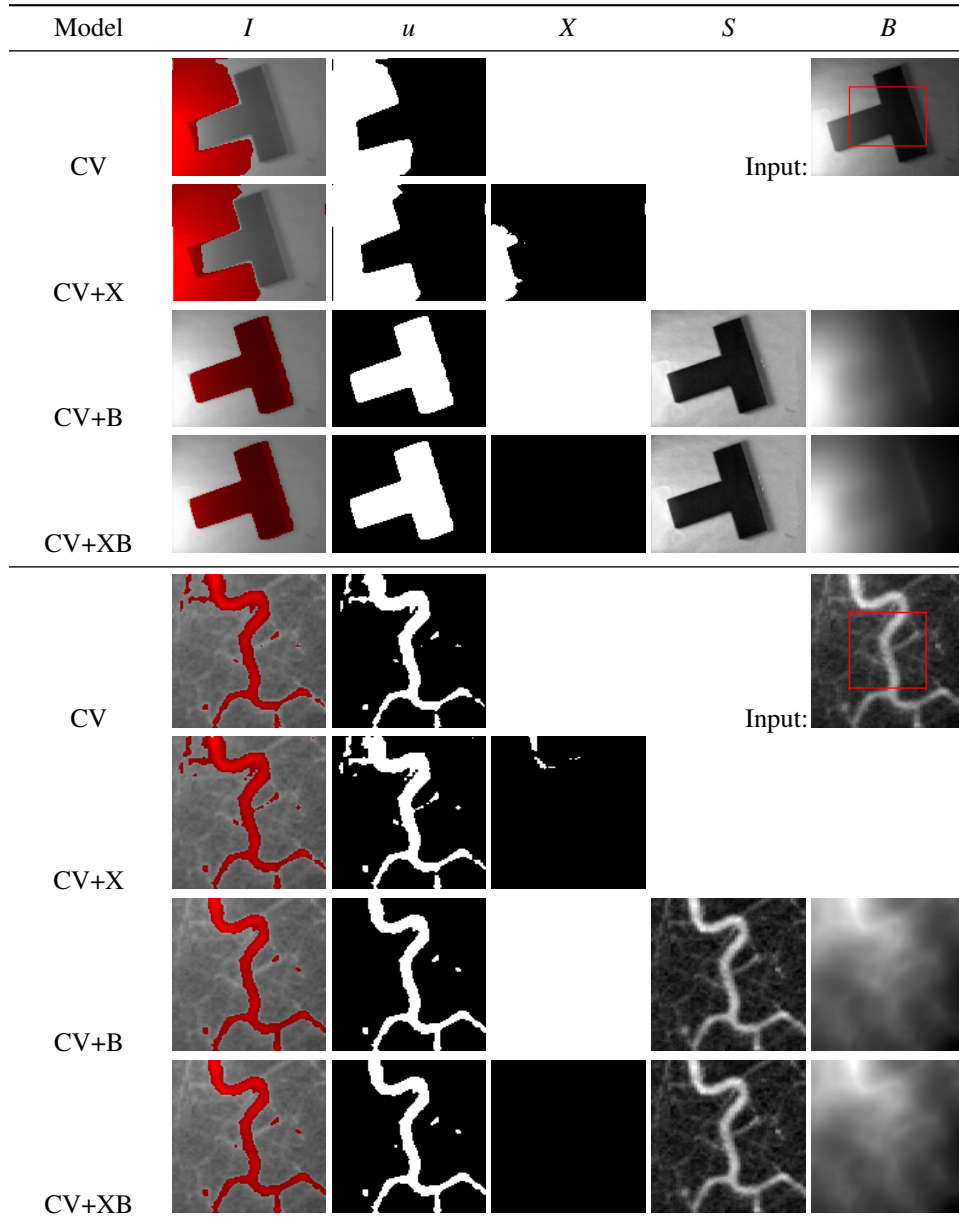| Model	I	u	X	S	B

FIGURE 2. Example cases 3 & 4. **Top:** The seemingly simple scene is not segmentable by the CV model alone, due to strong bias. CV+X wrongly classifies bright regions as artifacts. Bias correction (CV+B) results in accurate segmentation of the T-object. **Bottom:** The vessel structure is not accurately segmented by classical CV: superior parts are oversegmented due to brightening, inferior parts are undersegmented due to darkening. CV+X is inappropriate, while CV+B fixes the problem and leads to much improved vessel segmentation.

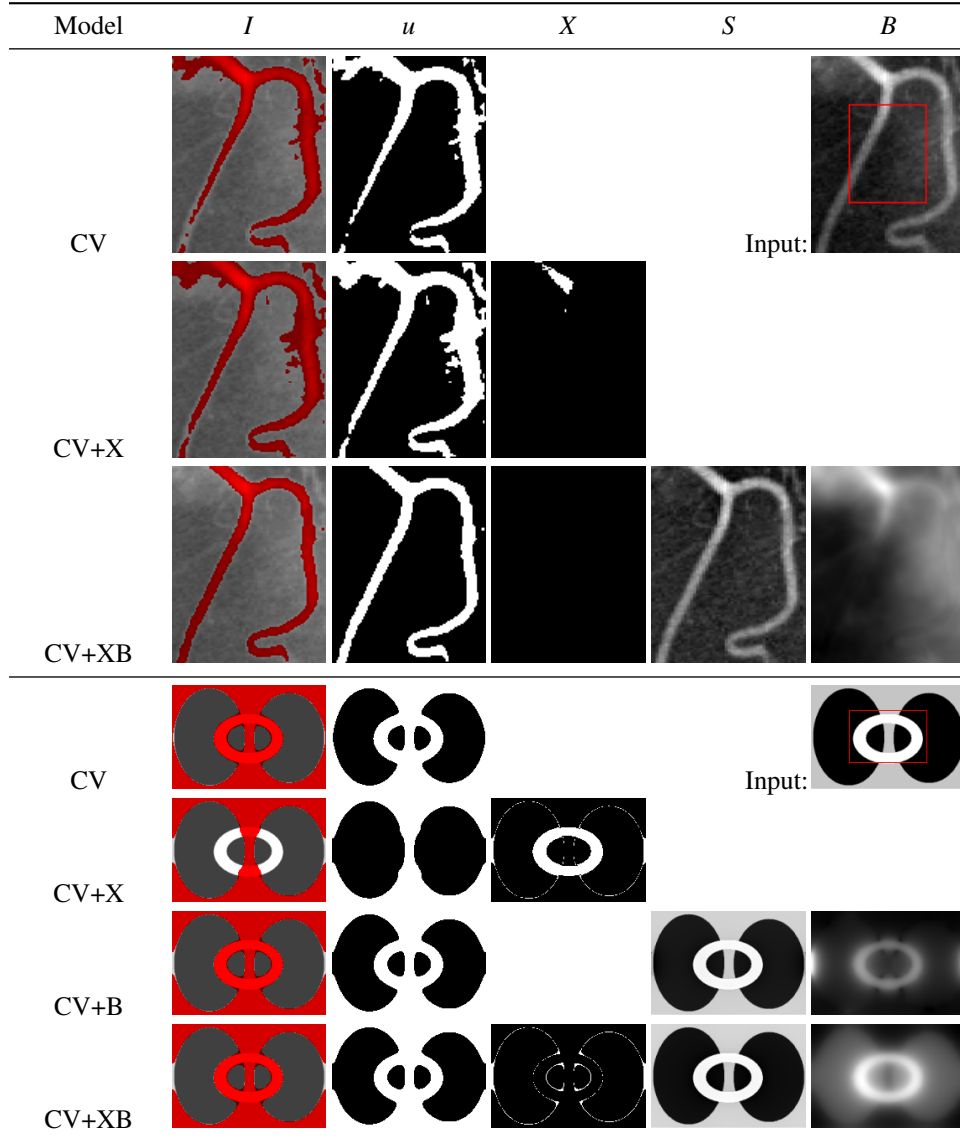| Model	*I*	*u*	*X*	*S*	*B*

FIGURE 3. Example cases 5 & 6. **Top:** Compare to ex. 4 in figure 2. **Bottom:** Three-phase piecewise constant synthetic image. The goal is to separate the two black ellipses from the gray background, considering the white ring to be an occlusion artifact. CV, however, groups the white ring with the light background. CV+X successfully identifies the ring as artifact, and closes the black ellipses thanks to the interface regularization. The bias correction is misleading, since much of the white ring will be considered overly illuminated background (CV+B, CV+XB), the corners being captured as transient artifacts (CV+XB).

FIGURE 4. Microscopy example cases. **Top:** This AFM image is severely affected by inhomogeneity compared to pattern contrast. As a result, classical CV segmentation fails. The proposed CV+XB model is able to capture some of the bias as such, and correctly segments some of the actual pattern. The central-square contour initialization, however, provokes an incorrect bias field estimate at early stages of the optimization, and leads to an incorrect local minimum, misclassifying the central portions. **Middle:** Starting from a near-optimal contour initialization of a single pattern element, the CV model still fails entirely. The proposed CV+XB model is not misled into incorrect minima, anymore, and successfully separates bias from actual pattern contrast. **Bottom:** The CV+XB model captures most of the inhomogeneity present in this AFM sample image and leads to reasonable segmentation of the diamond pattern. (Note: The inversion of foreground/background between CV and CV+XB models is arbitrary and triggered by domain size.)
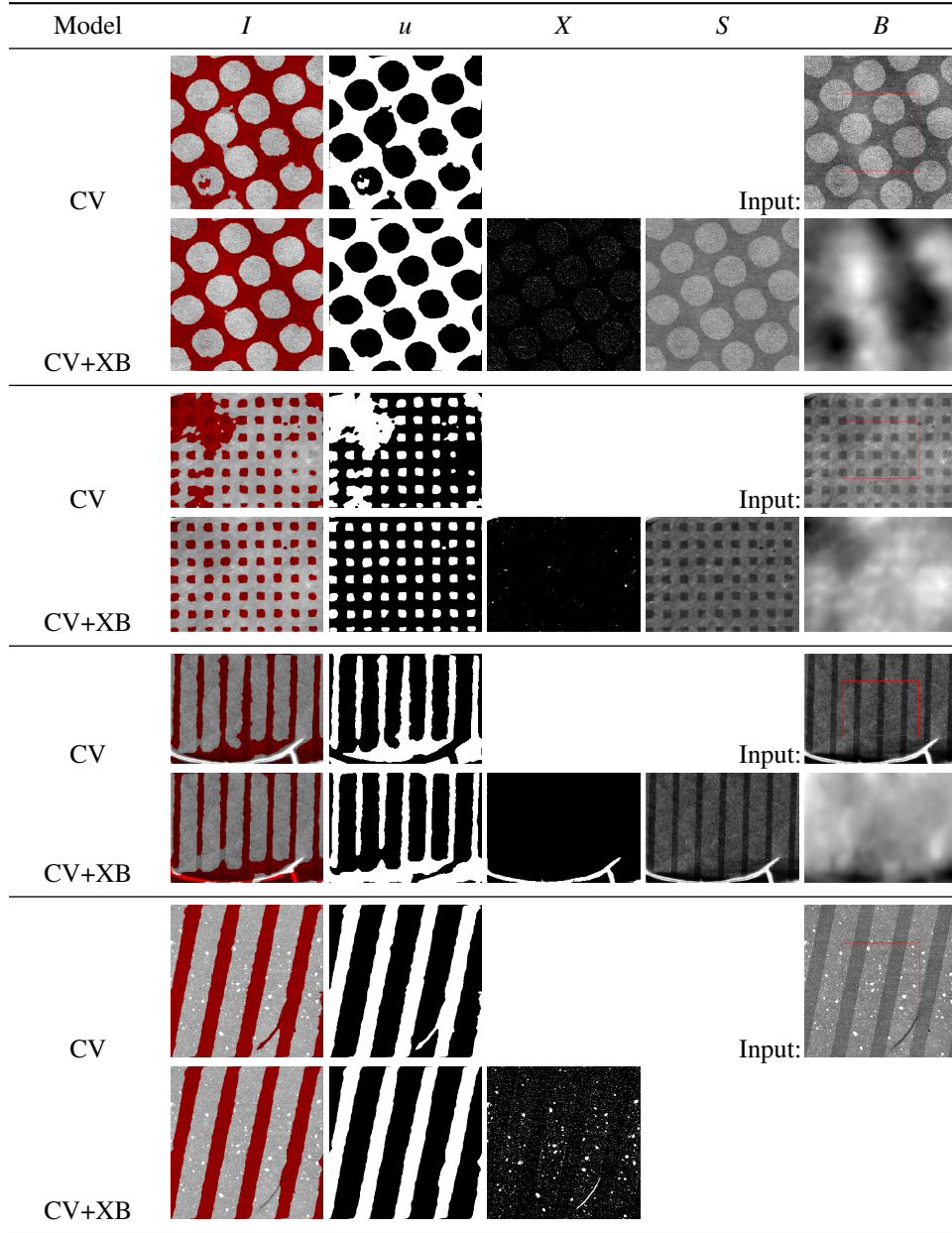
Model	I	u	X	S	B

FIGURE 5. Further microscopy examples. **Top:** Seemingly "easy" AFM sample, actually affected by strong inhomogeneity at different scales. CV+XB yields a flattened structural image and correct pattern segmentation. **Second row:** Fluorescence microscopy image suffering from strong bias and artifacts, failing classical CV. CV+XB corrects bias and captures most artifacts. **Third row:** AFM sample with crack (white) and bend (darkening). The darkening is beyond recovery, but the crack is correctly identified as artifact. **Bottom:** Artifact detection collects bright spots and the dark line, resulting in correct stripe-pattern segmentation.

associated with the constrained functional optimization by iterating several steps of co-ordinate descent and dual ascent. The resulting subproblems have closed form solutions (region statistics μ_1, μ_2, artifacts map X, and structure and bias field decomposition S and B, respectively), or admit efficient gradient descent/ascent steps (segmentation phase-field u, through modified MBO, and dual update λ). The proposed algorithm typically converges in about 10 to 50 iterations and takes fractions of a second on standard computing equipment.

Practical results from disparate imaging modalities illustrate the range of images that are successfully modeled by our joint energy functional. Finally, the MATLAB code implementing our algorithm and that produces the results presented in this paper is made available at http://www.math.ucla.edu/~zosso/code.html and at MATLAB Central.

REFERENCES

[1] A. Ayvaci, M. Raptis and S. Soatto, Sparse occlusion detection with optical flow, *International Journal of Computer Vision*, **97** (2011), 322–338.

[2] X. Bresson and T. F. Chan, Active contours based on Chambolle's mean curvature motion, in *2007 IEEE International Conference on Image Processing*, vol. 1, IEEE, 2007, I – 33–I – 36.

[3] X. Bresson, S. Esedoglu, P. Vandergheynst, J.-P. Thiran and S. Osher, Fast global minimization of the active contour/snake model, *Journal of Mathematical Imaging and Vision*, **28** (2007), 151–167.

[4] T. Brox and D. Cremers, On local region models and a statistical interpretation of the piecewise smooth Mumford-Shah functional, *International Journal of Computer Vision*, **84** (2008), 184–193.

[5] V. Caselles, R. Kimmel and G. Sapiro, Geodesic active contours, *Int. J. Comput. Vis.*, **22** (1997), 61–79.

[6] A. Chambolle, An algorithm for mean curvature motion, *Interfaces and Free Boundaries*, **6** (2004), 195–218.

[7] T. F. Chan and L. A. Vese, Active contours without edges, *IEEE Transactions on Image Processing*, **10** (2001), 266–277.

[8] T. Chan and W. Zhu, Level set based shape prior segmentation, in *CVPR 2005*, vol. 2, IEEE, 2005, 1164–1170.

[9] T. F. Chan, S. Esedoglu and M. Nikolova, Algorithms for finding global minimizers of image segmentation and denoising models, *SIAM Journal on Applied Mathematics*, **66** (2006), 1632–1648.

[10] T. F. Chan, B. Sandberg and L. A. Vese, Active contours without edges for vector-valued images, *Journal of Visual Communication and Image Representation*, **11** (2000), 130–141.

[11] R. Courant, K. Friedrichs and H. Lewy, Über die partiellen Differenzengleichungen der mathematischen Physik, *Mathematische Annalen*, **100** (1928), 32–74.

[12] D. Cremers, S. J. Osher and S. Soatto, Kernel density estimation and intrinsic alignment for shape priors in level set segmentation, *International Journal of Computer Vision*, **69** (2006), 335–351.

[13] D. Cremers, N. Sochen and C. Schnörr, A multiphase dynamic labeling model for variational recognition-driven image segmentation, *International Journal of Computer Vision*, **66** (2006), 67–81.

[14] S. Esedoglu and Y. H. R. Tsai, Threshold dynamics for the piecewise constant Mumford-Shah functional, *Journal of Computational Physics*, **211** (2006), 367–384.

[15] V. Estellers, D. Zosso, R. Lai, S. Osher, J.-P. Thiran and X. Bresson, Efficient algorithm for level set method preserving distance function, *IEEE transactions on image processing : a publication of the IEEE Signal Processing Society*, **21** (2012), 4722–34.

[16] P. Filzmoser, R. G. Garrett and C. Reimann, Multivariate outlier detection in exploration geochemistry, *Computers & Geosciences*, **31** (2005), 579–587.

[17] B. K. Horn, Determining lightness from an image, *Computer Graphics and Image Processing*, **3** (1974), 277–299.

[18] M. Jung, M. Kang and M. Kang, Variational image segmentation models involving non-smooth data-fidelity terms, *Journal of Scientific Computing*, **59** (2013), 277–308.

[19] M. Kass, A. Witkin and D. Terzopoulos, Snakes: Active contour models, *International Journal of Computer Vision*, **1** (1988), 321–331.

[20] R. Kimmel, M. Elad, D. Shaked, R. Keshet and I. Sobel, A variational framework for Retinex, *International Journal of Computer Vision*, **52** (2003), 7–23.

[21] E. H. Land, The Retinex, *American Scientist*, **52** (1964), 247–253,255–264.

[22] E. H. Land, The Retinex theory of color vision, *Scientific American*, **237** (1977), 108–128.

[23] E. H. Land and J. J. McCann, Lightness and Retinex theory, *Journal of the Optical Society of America*, **61** (1971), 1–11.

[24] C. Li, C.-Y. Kao, J. C. Gore and Z. Ding, Minimization of region-scalable fitting energy for image segmentation, *IEEE Transactions on Image Processing*, **17** (2008), 1940–1949.

[25] C. Li, C. Xu, C. Gui and M. D. Fox, Level set evolution without re-initialization: a new variational formulation, in *IEEE CVPR*, vol. 1, IEEE, 2005, 430–436, URL http://ieeexplore.ieee.org/xpl/freeabs_all.jsp?arnumber=1467299.

[26] C. Li, C. Xu, C. Gui and M. D. Fox, Distance regularized level set evolution and its application to image segmentation, *IEEE Transactions on Image Processing*, **19** (2010), 3243–3254.

[27] C. Li, C. Xu, K. M. Konwar and M. D. Fox, Fast distance preserving level set evolution for medical image segmentation, in *International Conference on Control, Automation, Robotics and Vision*, IEEE, 2006, 1–7.

[28] W. Ma and S. Osher, A TV Bregman iterative model of Retinex theory, 2010.

[29] B. Merriman, J. K. Bence and S. J. Osher, Motion of multiple junctions: a level set approach, *Journal of Computational Physics*, **112** (1994), 334–363.

[30] L. Modica, The gradient theory of phase transitions and the minimal interface criterion, *Archive for Rational Mechanics and Analysis*, **98** (1987), 123–142.

[31] J.-M. Morel, A.-B. Petro and C. Sbert, A PDE formalization of Retinex theory, *IEEE Transactions on Image Processing*, **19** (2010), 2825–2837.

[32] D. Mumford and J. Shah, Optimal approximations by piecewise smooth functions and associated variational problems, *Communications on Pure and Applied Mathematics*, **42** (1989), 577–685.

[33] J. Nocedal and S. J. Wright, *Numerical optimization*, 2nd edition, Springer, Berlin, 2006.

[34] S. Osher and J. A. Sethian, Fronts propagating with curvature-dependent speed: algorithms based on Hamilton-Jacobi formulations, *Journal of Computational Physics*, **79** (1988), 12–49.

[35] M. Prastawa, E. Bullitt, S. Ho and G. Gerig, A brain tumor segmentation framework based on outlier detection, *Medical Image Analysis*, **8** (2004), 275–283.

[36] M. Rousson and N. Paragios, Shape priors for level set representations, in *ECCV 2002* (eds. A. Heyden, G. Sparr, M. Nielsen and P. Johansen), vol. 2351 of Lecture Notes in Computer Science, Springer Berlin Heidelberg, Berlin, Heidelberg, 2002, 78–92.

[37] S. Ruuth, Efficient algorithms for diffusion-generated motion by mean curvature, *Journal of Computational Physics*, **625** (1998), 603–625.

[38] L. S. Slaughter, Q. Yang, T. D. Young, H. H. Cao, A. C. Serino, D. Zosso, J. An, J. Stevick, N. Takaki, M. Weiss, A. L. Bertozzi, A. M. Andrews and P. S. Weiss, Transparent ultrathin gold chemically patterned onto polymer supports via organic monolayers, 2015.

[39] L. A. Vese and T. F. Chan, A multiphase level set framework for image segmentation using the Mumford and Shah model, *International Journal of Computer Vision*, **50** (2002), 271–293.

[40] L. Wang, C. Li, Q. Sun, D. Xia and C.-Y. Kao, Active contours driven by local and global intensity fitting energy with application to brain MR image segmentation, *Computerized medical imaging and graphics*, **33** (2009), 520–31.

[41] M. Yan, Restoration of images corrupted by impulse noise and mixed gaussian impulse noise using blind inpainting, *SIAM Journal on Imaging Sciences*, **6** (2013), 1227–1245.

[42] Y. Yang, C. Li, C.-Y. Kao and S. Osher, Split Bregman method for minimization of region-scalable fitting energy for image segmentation, in *Advances in Visual Computing*, vol. 6454 of Lecture Notes in Computer Science, Springer Berlin Heidelberg, 2010, 117–128.

[43] D. Zosso, G. Tran and S. Osher, A unifying Retinex model based on non-local differential operators, in *IS&T/SPIE Electronic Imaging* (ed. C. A. Bouman), 2013, 865702–1–16.

[44] D. Zosso, G. Tran and S. J. Osher, Non-local Retinex - a unifying framework and beyond, *SIAM J. Imaging Sciences*, **submitted**.

E-mail address: zosso@math.ucla.edu
E-mail address: anancheer@ucla.edu
E-mail address: jamesrstevick@gmail.com
E-mail address: ntakaki@andrew.cmu.edu
E-mail address: mweiss010@gmail.com
E-mail address: slaughter@chem.ucla.edu
E-mail address: serotonin@ucla.edu
E-mail address: psw@cnsi.ucla.edu
E-mail address: bertozzi@math.ucla.edu